A&A manuscript no.
(will be inserted by hand later)

Your thesaurus codes are:
3(11.19.2;11.09.4;09.04.1;09.08.1)

ASTRONOMY
AND
ASTROPHYSICS
5.2.2008

Dust extinction of H II regions in NGC 598 and NGC 5457 ⋆

L. Petersen and P. Gammelgaard

Institut for Fysik og Astronomi, Aarhus Universitet, Ny Munkegade, DK-8000 Århus C, Denmark

Received ; Accepted

Abstract. The dust extinction towards bright H II regions in NGC 598 and NGC 5457 has been studied in detail by forming line ratios of Balmer and Paschen emission lines covering a large wavelength range. Three homogeneous models of the geometrical distribution of the emitting sources and the obscuring dust have been tested. Only for low extinctions can the data be fit by a homogeneous slab. For most of the observed H II regions the Witt et al. (1992) 'dusty nucleus' model matches the observations equally well as the usual assumption of a foreground screen, but the former implies much larger actual dust contents. Spatial variations in the optical depth in V of the order 0.3 across a region are found.

Key words: galaxies: spiral – galaxies: ISM – dust, extinction – H II regions

1. Introduction

Investigations of external galaxies are often faced with the problem of disentangling the effects of dust and the physical properties, e.g. age, IMF, chemical composition etc. of the emitting source.

The effect of dust extinction goes roughly as λ^{-1} and will consequently change the observed spectral energy distribution. Studies and interpretation of the physical properties in external galaxies therefore rely on how well we can account for the attenuation of the emitted light due to dust. The wavelength dependence makes multiwavelength analyses favourable and a growing number of investigations combining optical and IR wavelengths have been made both using imaging (e.g. Jansen et al. 1994; Witt et al. 1994; Evans 1995; van Driel et al. 1995) and spectroscopy (e.g. Puxley & Brand 1994; Calzetti et al. 1996).

In the analysis of spectra of extragalactic H II regions the correction for dust extinction is usually made on the assumption that the intrinsic hydrogen emission line spectrum is known through case B recombination and any difference between the emergent and intrinsic flux ratios can be ascribed to dust obscuration following the Galactic extinction curve.

Throughout the years, the use of the ratio of the two strongest Balmer lines, Hα/Hβ, sometimes in combination with Hγ, has been prevailing, albeit they only span a limited wavelength range, because they will be included in almost any optical spectra and are easy to detect. It has long been proposed to expand the baseline for extinction determination by comparing near-IR hydrogen Paschen lines with emission lines from the Balmer series at short wavelengths (cf. Greve et al. 1989; Osterbrock 1989). Such line pairs are all separated by wide wavelength intervals over which the extinction has a large effect and is therefore potentially easier to deduce. Additionally, some line pairs form corresponding multiplet lines, Pn/Hn originating at the same upper atomic level with relative strength depending primarily on the transition probability and minimised dependence on theoretical recombination line calculations (Greve et al. 1994).

In Petersen & Gammelgaard (1996; hereafter Paper I) we have demonstrated the feasibility of observing lines from the Paschen series and the short end of the Balmer series from giant extragalactic H II regions simultaneously with a two-channel spectrograph. In the present paper we will further discuss dust extinction towards H II regions in NGC 598 and NGC 5457 as derived from spectra obtained with the same instrument.

The straightforward application of the Galactic interstellar extinction curve derived from point sources to extended emission regions in external galaxies is, however, problematic, because this procedure implicitly assumes a dust configuration of a homogeneous foreground absorbing screen. Intuitively one would expect things to be more complicated in reality with dust distributed in a patchy or clumpy way maybe mixed with the emitting source (Witt et al. 1992; hereafter WTC; Calzetti et al. 1994, 1996; Puxley & Brand 1994) and with scattering of, particu-

Send offprint requests to: larsp@obs.aau.dk

⋆ Based on observations collected at the Nordic Optical Telescope, La Palma, Spain

larly blue, photons into the line of sight by dust grains (Bruzual et al. 1988; WTC). This could all lead to a much greyer effective extinction curve than the standard Galactic curve. This was exemplified in Paper I by using an extinction curve with $R_{\rm V} = A_{\rm V}/E_{\rm B-V} = 6$, here we will address this issue by fitting three different models of relative spatial distribution of emitting source and dust to the measured line ratios.

2. The models

When data from a wide wavelength range are available it is possible to test various models for the geometrical distribution of the dust. Although the data presented here only reach Pδ at 1.0 μm and in two cases Pγ at 1.1 μm, they can still be used to test some basic models and have the advantage of being recorded simultaneously with the same instrument as the Balmer emission lines. Three models have been considered: (1) The naive but widely used uniform foreground extinction screen, (2) a slab model of homogeneous mixture of dust and emitting sources and (3) that of the WTC scenarios which best models an extragalactic H II region, the so-called "dusty nucleus".

The extinction can be quantified in many ways, e.g. as the logarithmic extinction at Hβ, C(Hβ), the visual extinction in magnitudes, $A_{\rm V}$ or as the optical depth in V, $\tau_{\rm V}$, depending on the purpose it is used for. In this work we will express the derived dust extinction as $\tau_{\rm V}$ for uniformity among the models. In the case of a foreground screen simple relations exist between these, with $\tau_{\rm V} = 1.98C({\rm H}\beta) = A_{\rm V}/1.086$.

Depending on the actual distribution the same total amount of dust can produce very different attenuation of the emitted light. Therefore we define an effective optical depth $\tau_{\rm eff} = -\ln(\mathcal{F}_{\rm obs}/\mathcal{F}_{\rm em})$. In most cases the actual optical depth will exceed $\tau_{\rm eff}$, thus some source distributions are capable of hiding away larges amount of extinguishing matter.

More complicated models with clumpiness could be included, but due to the lack of near-IR lines at longer wavelengths and the rather low extinction for some of the regions we do not find it justified to attempt to discriminate between clumpy and homogeneous distributions. Thus we limit ourselves to the three homogeneous models but it must be stressed that these will produce lower limits to the dust content as compared to corresponding clumpy models. Calculations of the effect on the emitted radiation field by a clumpy screen with dust-free interclump medium excluding scattering (Natta & Panagia 1984), a two-phase slab (Boissé 1990) and spherical two-phase clumpy systems with non-conservative scattering (Witt & Gordon 1996) all show reduced overall effective optical depth relative to homogeneous distributions of the same mass and flatter effective extinctions curves. As clumps will become optically thick much quicker than an equivalent homogeneous distribution would, a clumpy dust distribution will produce less reddening in a given geometry with an extended source distribution and approach lower finite limiting reddening with increasing dust mass (Witt & Gordon 1996). Thus the dust content derived on the assumption of homogeneous distributions can underestimate the true dust mass.

2.1. Foreground screen

This is the most simple geometry of dust distribution, inherited from stellar astronomy but likely to be invalid for many extragalactic studies where more complicated geometries are expected (WTC). On the other hand Calzetti et al. (1996) found evidence that it might be applicable for star burst environments, where large fractions of the dust have been depleted or ejected. By chance it happens to be the geometry where any amount of dust has the strongest effect on the emitted flux and taken at face value it will always yield a lower limit to the true dust content.

For any pair of emission lines the relationship of observed line flux ratio and the predicted ratio in the absence of dust is

$$\frac{R_{\rm o}}{R_{\rm p}} = {\rm e}^{\tau_{\lambda 2}-\tau_{\lambda 1}}. \quad (1)$$

Hence, as an exception, the foreground screen has by definition $\tau = \tau_{\rm eff}$. Introducing a normalised extinction curve $\tau_\lambda/\tau_{\rm V} = A_\lambda/A_{\rm V}$ one can solve for $\tau_{\rm V}$

$$\tau_{\rm V} = \frac{\ln(R_{\rm o}/R_{\rm p})}{\tau_{\lambda 2}/\tau_{\rm V} - \tau_{\lambda 1}/\tau_{\rm V}} \text{ or } A_{\rm V} = \frac{2.5\log(R_{\rm o}/R_{\rm p})}{A_{\lambda 2}/A_{\rm V} - A_{\lambda 1}/A_{\rm V}}, \quad (2)$$

if transforming to magnitude. The first expression in Eq. (2) is of cause the motivation for illustrating the data as in Fig. 2–4.

2.2. Homogeneous slab

A slab model of mixture of dust and emitting sources may resemble the actual geometry better than the overlying screen in some cases, although a single or a few knots of emission surrounded by non-uniform dust is probably the dominating picture. For a homogeneous mixture throughout neglecting scattering $R_{\rm o}/R_{\rm p}$ can be described in terms of the optical depth (Disney et al. 1982, Puxley & Brand 1994)

$$\frac{R_{\rm o}}{R_{\rm p}} = \frac{\tau_{\lambda 2}}{\tau_{\lambda 1}}\left(\frac{1-{\rm e}^{-\tau_{\lambda 1}}}{1-{\rm e}^{-\tau_{\lambda 2}}}\right) \quad (3)$$

When introducing relative values $\tau_\lambda/\tau_{\rm V}$ we end up with the only free parameter $\tau_{\rm V}$, which is fit to give the best match to the data points.

2.3. Dusty nucleus

This is probably the most realistic model of the real dust distribution affecting the emitted flux from an H II region. The WTC 'dusty galactic nucleus' environment consists of a dust-free spherical source surrounded by a dust-shell without emitting sources and is characterised by the optical thickness of the shell, τ_V. The main difference between this model and the other two is the presence of a dust-shell subtending a large solid angle as seen by the source and the inclusion of scattered light back into the line of sight from it, whereas the other models only include pure extinction (absorption and scattering out of the line of sight). This difference has increasing impact in the short-wavelength end resulting in a 'bluing' of the spectrum partly cancelling the reddening effect of the extinction and leading to a flatter effective extinction curve. Consequently, the observational effect will be to see values of $\ln(R_o/R_p)$ close to zero in the blue end of Figs. 2–4 even at large optical depths in contrast to the two other distributions, which lead to decreasing values of $\ln(R_o/R_p)$ as function of τ_λ/τ_V with a slope depending on τ_V.

WTC tabulate the amount of direct and scattered light received at the central wavelength of the broad band colours calculated from Monto Carlo simulations of the transfer of radiation. In this analysis we have interpolated their tables to the wavelength of the relevant emission lines by cubic splines and use the sum of the two contributions as the observed flux.

3. Observations

The spectra were obtained with the Århus-Tromsø Low Dispersion Spectrograph at the Nordic Optical Telescope, La Palma on July 31 and August 1 1994, together with some of the data presented in Paper I.

Three extended H II regions in NGC 598 all classified as extremely strong by Boulesteix et al. (1974) were observed. NGC 604 is the largest H II region in NGC 598 and resembles in some respect the 30 Dor complex in the LMC. The elemental abundance has been studied in detail by Díaz et al. (1987) using multiple slit positions. We have positioned the slit in an E-W direction through the center of the complex and extracted spectra from three bright knots roughly coinciding with their areas denoted D, B and C. In NGC 595, another large region, the slit was positioned across the southern part. B88 shows a feeble ring-like structure and one spectrum on the east and west side of the ring was extracted.

The five H II regions observed in NGC 5457 are all situated in the south-east part of the galactic disk. The giant complex NGC 5461 was observed in two slit positions both centered visually on the peak luminosity from short Hα-exposures. One position (Jul 31) is E-W while the other is roughly in the NE-SW direction to include H1026 and H1117 with NGC5461. A complete log of the observations is given in Table 1.

Table 1. Journal of observations

Date	Galaxy	H II reg.[a]	Apertures ($''$)	Total exp. (s)
Aug 1	NGC 598	N595	2.2×33.4	3600
Aug 1	NGC 598	B88	2.2×8.3	3600
			2.2×8.3	3600
Aug 1	NGC 598	N604	2.2×9.2	1800
			2.2×7.5	1800
			2.2×8.3	1800
Jul 31	NGC 5457	N5461	2.2×15.8	3600
Jul 31	NGC 5457	H949	2.2×10.8	1800
		H961	2.2×8.3	1800
Aug 1	NGC 5457	H1026	2.2×8.3	6000
		N5461	2.2×10.0	6000
		H1117	2.2×9.2	6000

[a] ID numbers from Boulesteix et al. (1974) and Hodge et al. (1990) are preceded by B and H, respectively

During both nights the spectrophotometric standard star BD +17°4708 (Oke & Gunn 1983) was observed multiple times. For all H II regions and the standard star the blue and near-IR spectral ranges were observed simultaneously in the blue and red channel of the spectrograph to ensure precise relative spectrophotometry of the Balmer and Paschen lines. The two channels have dispersions of 2.0 Å/pixel and 7.5 Å/pixel and cover 3950–4900 Å and 8000–11000 Å, respectively. A detailed description of the instrument and observation and reduction procedures can be found in Paper I.

3.1. Data reduction

All the CCD exposures were reduced with standard IRAF packages for flat fielding, calibrations and extraction of the one-dimensional spectra. Rectification of the two-dimensional frames and transformation to a common spatial coordinate system were done with a special slit mask as explained in Paper I.

In the combined object frames extraction apertures were set to enclose each distinct emission region; the resulting apertures are listed in Table 1. The sky background was sampled along large part of the slit, avoiding any sign of emission, to get a good S/N of the sky subtraction in the near-IR.

3.2. Relative line fluxes

In Fig. 1 we present an example of the final flux calibrated spectra in the blue and near-IR wavelength range from of one of the H II regions with high signal. The line fluxes have been measured by fitting Gaussian profiles to the line

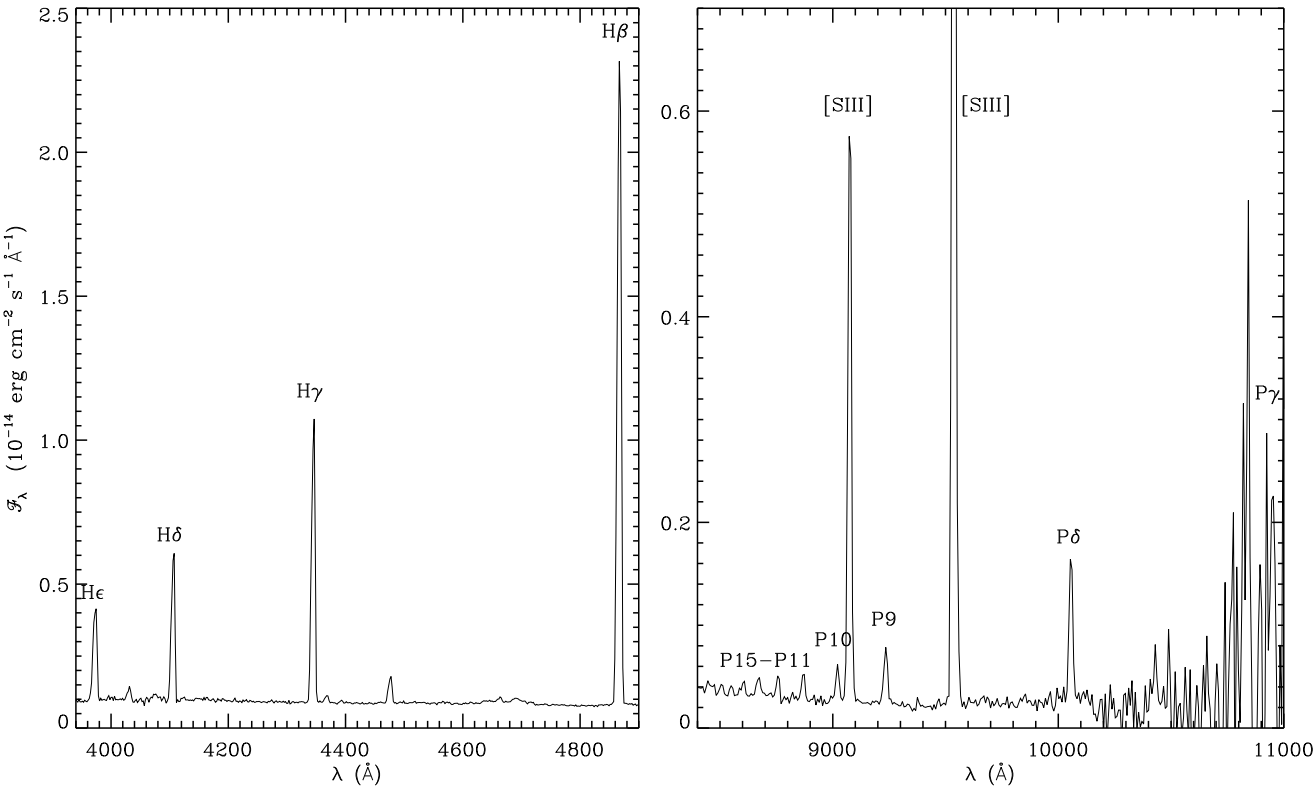

Fig. 1. Left panel, Blue spectrum of NGC 5461 showing four strong Balmer emission lines. Right panel, near-IR spectrum of the same region. The Paschen lines P15–Pγ are clearly identified, although with rapidly increasing noise for $\lambda > 10500$ Å. Note the different scales on the axes

profiles or two Gaussians when deblending Hϵ from the nearby [Ne III] line. As evident from Fig. 1 the spectrum has low S/N at the position of Pγ. This line was only detected in two of the spectra and the flux could not in any case be determined from the IRAF procedure. Instead the flux was measured by fitting a Gaussian with fixed λ_0.

For the strong Balmer lines we estimate the accuracy of the flux measurements to be of the order 5 %. Because Hϵ is measured from a deblending procedure it has a larger flux of error estimated to 20 %. In the near-IR flux uncertainties are dominated by the more critical sky subtraction and determination of the spectral continuum level. At P15 we tend to reach the series limit where the faint Paschen lines start to blend giving rise to a false continuum, this line is therefore excluded from the present analysis. Judged upon the line profile fitting procedure we assign an error estimate of 20 % to the two faintest lines included (P14 and P13) and to P9, which is strongly affected by the atmospheric H_2O absorption band, and half of this to P12–P10 and Pδ.

The nebular Balmer emission lines are affected by the absorption lines in the underlying stellar spectrum. This will suppress the observed flux of the lines and relative more so at the short end of the line series, thus partly counteracting the effect of scattering on dust grains. The exact correction for underlying Balmer absorption is very uncertain, because it depends on the actual stellar population and age. Due to the lack of any detailed knowledge we have decided to use the average absorption equivalent width of 1.9 Å, found by McCall et al. (1985), for all Balmer lines. A similar value was found by Díaz et al. (1987) in their analysis of NGC 604. In most cases the correction is quite small and will be less than the quoted error bars, except for Hδ in the faintest regions and at Hϵ, where it may constitute a fair fraction of the measured line flux. We deal with this problem by assigning errors to include no correction and corrections up to 4 Å equivalent width in a fashion similar to Puxley & Brand (1994). The large uncertainty for some of the spectra further cautions the usage of Hϵ.

In Table 2 we list the line flux relative to Hβ of all identified hydrogen emission lines of the observed H II regions in NGC 598 and NGC 5457.

4. Discussion

The quotient of observed and predicted line fluxes in three of the observed regions relative to Hβ,

$$\frac{R_{\rm o}}{R_{\rm p}} = \left(\frac{\mathcal{F}(\lambda)}{\mathcal{F}(\mathrm{H}\beta)}\right)_{\rm o} \Bigg/ \left(\frac{I(\lambda)}{I(\mathrm{H}\beta)}\right)_{\rm p} \quad (4)$$

Table 2. Observed line fluxes (normalised at $\mathcal{F}(\mathrm{H}\beta) = 1$)

ID	$R_\mathrm{o} = \left(\frac{\mathcal{F}(\lambda)}{\mathcal{F}(\mathrm{H}\beta)}\right)_\mathrm{o}$											
	N595	B88,1	B88,2	N604,1	N604,2	N604,3	N5461	H949	H961	H1026	N5461	H1117
Hϵ	0.102	0.130	0.122	0.137	0.125	0.096	0.104	0.122	0.098	0.091	0.101	0.188
Hδ	0.232	0.235		0.253	0.256	0.252	0.209	0.210	0.212	0.178	0.191	
Hγ	0.409	0.437	0.491	0.441	0.456	0.451	0.392	0.402	0.395	0.387	0.365	0.370
Hβ	1.000	1.000	1.000	1.000	1.000	1.000	1.000	1.000	1.000	1.000	1.000	1.000
P14	0.011			0.010	0.009		0.016					
P13	0.019	0.009		0.013	0.012		0.020				0.022	
P12	0.023	0.014	0.013	0.014	0.015		0.020				0.034	
P11	0.029	0.015	0.020	0.017	0.018		0.025				0.039	
P10	0.048	0.022	0.044	0.021	0.021	0.029	0.035		0.049	0.062	0.039	0.115
P9	0.064	0.034	0.052	0.038	0.037	0.055	0.059	0.057	0.068	0.110	0.071	0.126
Pδ	0.159	0.085	0.164	0.090	0.101	0.064	0.158	0.145	0.200	0.360	0.211	
Pγ					0.378		0.297					
$\mathcal{F}\,(\mathrm{H}\beta)^a$	-12.55	-13.07	-13.48	-12.43	-12.61	-13.59	-12.73	-13.38	-13.50	-13.90	-12.79	-14.43

[a] Logarithm of the Hβ-flux in units of erg cm^{-2} s^{-1}

are plotted in Figs. 2–4 with $\tau_\lambda/\tau_\mathrm{V} = A_\lambda/A_\mathrm{V}$ on the abscissa as derived from the fitting formula by Cardelli et al. (1989) with the standard value $R_\mathrm{V} = 3.1$. The choice of normalising to Hβ is simply a matter of convenience and when deriving τ_V from the corresponding multiplet lines the relevant Balmer lines are used in the general expression Eq. (2).

The theoretical line ratios R_p for case B recombination are adopted from Hummer & Storey (1987). The electron temperature and density have been determined by Kwitter & Aller (1981), Rayo et al. (1982), Díaz et al. (1987) and Vílchez et al. (1988). For the two regions (H1026 and H1117) where T_e and n_e can not be acquired from the literature we used typical values of 10^4 K and 10^2 cm^{-3} and include realistic variations in the error estimates in Tables 3 and 4. The weak variation of R_p with these parameters will in any case only introduce uncertainties smaller than the expected observational errors (Greve et al. 1994).

According to Eq. (2) the overlying screen will manifest itself as a straight line with a slope equal to $-\tau_\mathrm{V}$ in this type of plot. Figure 2 illustrates this for NGC 5461. The best linear fit to the data points gives $\tau_\mathrm{V} = 1.04$ (Table 3) with $\chi^2 = 13$, but fails to match the data points at the longest wavelengths, i.e. smallest $\tau_\lambda/\tau_\mathrm{V}$. More complicated geometries introduce curvature in the plots (see Eq. (3) and Figs. 2–3). A homogeneous slab with optical depth $\tau_\mathrm{V} = 4.3$ fits the data equally well or perhaps even better ($\chi^2 = 11$), especially at the long wavelength end. The 'dusty nucleus' model of $\tau_\mathrm{V} = 3$ does not fit quite as well ($\chi^2 = 34$). Although it gives a good match to Pγ and Pδ it exaggerates somewhat the 'blueing' of the spectrum at short wavelengths caused by scattering. Bearing the problems of the Hϵ line flux in mind this might not be significant, though.

Given the indicated uncertainties it would be wrong to rule out any of the analysed dust configurations for this particular H II region, but it is clearly demonstrated that while the more complex dust geometries have effective optical depths only moderately higher than a foreground screen the true dust content can be as much 3–4 times higher. A definite discrimination of various models will need observations of emission lines in the Paschen and Brackett series at still longer near-IR wavelengths (Puxley & Brand 1994).

From the observation of NGC 5461 in the other slit position the following night we derive larger values of the optical depth, $\tau_\mathrm{V} = 1.41$ for the foreground screen and $\tau_\mathrm{V} = 5$ for the 'dusty nucleus'. No acceptable fit was produced by the homogeneous slab model. This deviation is larger than the estimated uncertainties and we believe it is real and a consequence of the non-coinciding slit positions, and only partly attributable to the effect of differential refraction (Filippenko 1982) and the overall lower signal, since the principal Paschen lines all stand well out of the noise level of the continuum and the slit is much larger than the typical seeing encountered during the observations ($< 1''$) and was close to the optimal orientation. As discussed in section 4.1 variations of this order of magnitude are likely to be present across giant H II regions at the spatial scale sampled here.

The optical depths for all the H II regions observed in NGC 5457 deduced from the three different dust distributions are collected in Table 3. H949 is the only other region where it was possible to obtain a best fitting model from the homogeneous slab distribution with $\tau_\mathrm{V} < 10$.

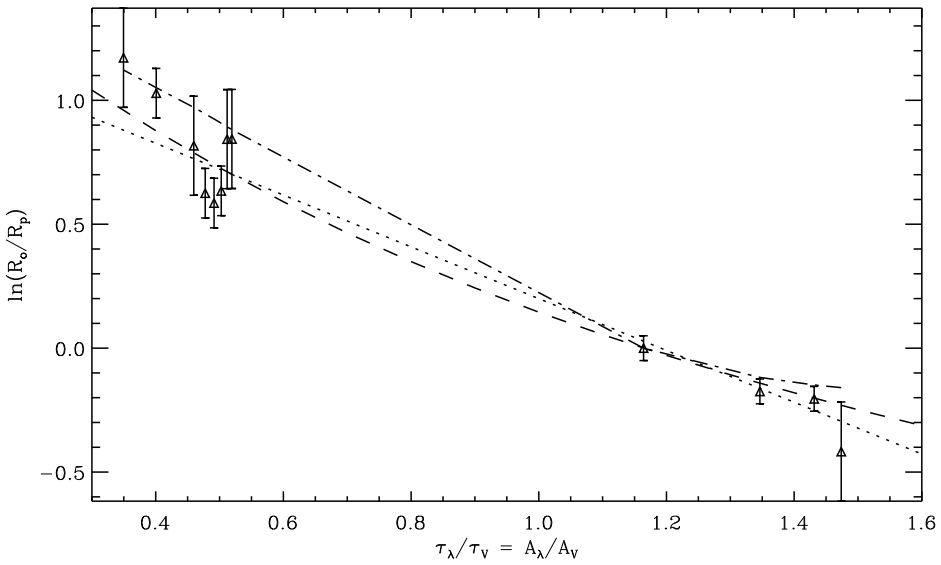

Fig. 2. Observed and predicted line flux relative to Hβ in the H II region NGC5461 with three best fit models for the dust distribution: Foreground screen (dotted line), homogeneous slab (dashed line) and the WTC 'dusty nucleus' (dot-dashed)

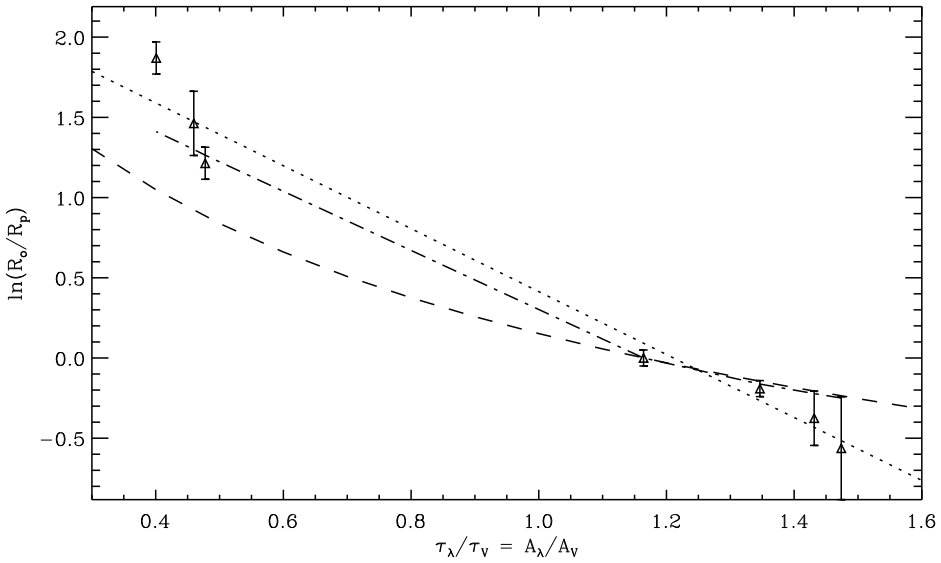

Fig. 3. Same as Fig. 2 but for the region H1026 where the quotients of observed and predicted line ratios clearly cannot be fit by the homogeneous slab model

(For larger values of τ_V the slab model have an asymptotic behaviour which will not change the shape of the curve with increasing optical depth.) The data from this H II region are also well fit with a 'dusty nucleus' model of $\tau_V = 3$. For H1026 and H1117 we find remarkable high values of the optical depth that obviously cannot be fit by the homogeneous slab (see Fig. 3), and is best described by a WTC model with τ_V equal 4 or 5, suggesting that quite large amounts of dust are associated with the spiral arm along which these two regions are positioned.

In Fig. 4 we plot the relative line fluxes of NGC 604 in NGC 598 in the same fashion as for NGC 5461. Since Pγ is just barely identified it has not been included in the diagram. Evidently, this H II region experiences much less dust extinction making it even harder to distinguish between any of the three models. The plotted curves fit the data points equally well with both the homogeneous slab model and the 'dusty nucleus' model having $\tau_V = 1$, but apparently the scattering properties of the WTC model follow better the flattening of $\ln(R_o/R_p)$ for the blue optical lines. None of the models adequately fit the measurement of Pδ, which indicate higher extinction.

Table 4 lists the values of the optical depth derived from the three models for the observed H II regions in NGC 598. In general they show low values of τ_V with the highest found for NGC 595. For this H II region the observations are best described by a homogeneous slab or the 'dusty nucleus' model again with indications of a 'blueing' of the spectrum at short wavelengths. For the other observations none of the considered models stand out.

Two pairs of corresponding multiplet lines, Pγ/Hδ and Pδ/Hϵ, are included in the present observations but the former only for two of the H II regions. While the usage of any of the two pairs are not unproblematic and involve

Table 3. Optical depth τ_V for the observed H II regions in NGC 5457 , a '–' indicate that no acceptable fit could be obtained. The Galactic extinction is 0. in this direction (de Vaucouleurs et al. 1991)

	N5461	H949	H961	H1026	N5461	H1117
Foreground screen						
Pγ/Hδ	1.27 ± 0.2					
Pδ/Hϵ	1.35 ± 0.2	1.14 ± 0.3	1.65 ± 0.2	2.27 ± 0.3	1.65 ± 0.2	
Pδ/Hβ	1.35 ± 0.2	1.26 ± 0.2	1.68 ± 0.2	2.45 ± 0.2	1.73 ± 0.2	
linear fit	1.04 ± 0.07	1.15 ± 0.06	1.31 ± 0.10	1.96 ± 0.2	1.44 ± 0.09	2.26 ± 0.3
Homogenous slab	4.3	5.5	–	–	–	–
Homogenous slab, eff	1.5	1.7	–	–	–	–
WTC	3	3	3	4	3	5
WTC, eff	1.7	1.7	1.7	2.4	1.7	3.1
Peimbert & Spinrad (1970)	0.40 ± 0.1				0.40 ± 0.10	
Smith (1975)	0.83				0.83	
Rayo et al. (1982)	1.49	(1.39)			1.49	
McCall et al. (1985)	1.16 ± 0.13				1.16 ± 0.13	
Kennicutt & Garnett (1996)	0.71 ± 0.10	0.77 ± 0.06		0.22 ± 0.04	0.71 ± 0.10	
Skillman & Israel (1988)[a]	1.23				1.23	
Rosa & Benvenuti (1994)[b]	0.87				0.87	

[a] Derived from the Brγ/Hβ ratio
[b] Based on HST observations and population models

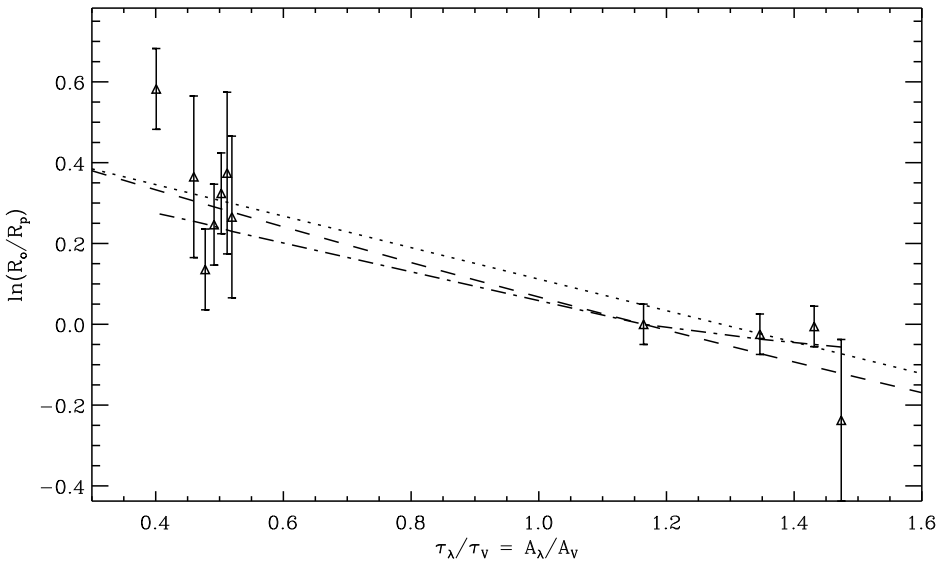

Fig. 4. As Fig. 2 but for the central emission region of the NGC 604 complex

large flux uncertainties they do on the other hand provide the advantage of common upper levels and less reliance on the recombination models. Here they have been included in Tables 3 and 4 for reason of comparison with derivations based on all observed emission lines. It is evident that ratios of these Paschen and Balmer lines always yield a higher value of τ_V, although with larger errors than using the full set of observed lines. This could be due to an underestimation of the Hϵ flux in the deblending process and the correction for underlying Balmer absorption or the low S/N at the position of Pγ reflected in the quoted error bars. But Figs. 2 and 4 also show that Pγ and Pδ always lie above the straight line outlined by the remaining points, thereby indicating some curvature away from the foreground screen model. This higher optical depth determined from emission lines with long wavelength baselines is further discussed in section 4.2.

Finally, we have included extinction calculations based on the single line pair made up of the Paschen and Balmer line with highest S/N, namely Pδ/Hβ. The derived optical depths from this ratio agrees well with those found on the basis of the corresponding line pair Pδ/Hϵ, expect

Table 4. Optical depth τ_V for the observed H II regions in NGC 598. $\tau_V^{Gal} = 0.13$ (de Vaucouleurs et al. 1991)

	N595	B88,1	B88,2	N604,1	N604,2	N604,3
Foreground screen						
Pγ/Hδ					1.31 ± 0.4	
Pδ/Hϵ	1.38 ± 0.2	0.54 ± 0.4	1.22 ± 0.3	0.57 ± 0.2	0.76 ± 0.2	0.59 ± 0.3
Pδ/Hβ	1.35 ± 0.2	0.52 ± 0.2	1.38 ± 0.2	0.62 ± 0.2	0.76 ± 0.2	0.18 ± 0.2
lin. fit	1.08 ± 0.08	0.32 ± 0.06	0.87 ± 0.15	0.35 ± 0.06	0.39 ± 0.09	0.41 ± 0.14
Homogenous slab	6.5	0.8	3.8	0.9	1.0	1.0
Homogenous slab, eff	1.9	0.4	1.4	0.4	0.5	0.5
WTC	3	1	2	1	1	1
WTC, eff	1.7	0.5	1.1	0.5	0.5	0.5
Peimbert & Spinrad (1970)				(	0.44 ± 0.10	)
Smith (1975)	1.00			(	0.	)
French (1980)				(	0.80	)
Kwitter & Aller (1981)	1.35	(0.50)		(	0.75	)
McCall et al. (1985)	0.95					
Díaz et al. (1987)				0.59	0.59	0.79
Melnick et al. (1987)	0.77			(	0.59	)
Vílchez et al. (1988)		(0.20)		(	0.69	)

in the case of N604,3 due to the very small Hϵ flux measured for this region. For the faintest regions Pδ/Hβ gives a smaller formal uncertainty than the corresponding line pairs, but generally the uncertainties are of the same size since Pδ/Hβ has a somewhat smaller separation.

What changes to the derived physical properties of the H II regions does the choice of extinction model make? This will depend on the wavelengths and strengths of the relevant lines, but since the effective optical depths do not differ very much among the models it is not expected to see large effects on derived physical parameters. This can be illustrated by the oxygen abundance calibrator $R_{23} = ([\mathrm{O\,II}] + [\mathrm{O\,III}])/\mathrm{H}\beta$ widely used to determine the metallicity of spiral galaxies. For this ratio the main difference will be on the [O II] lines due to the scattering included in the WTC model, while [O III] only will experience minute changes relative to Hβ.

From the uncorrected line fluxes of NGC 604 by Diaz et al. (1987) we have calculated the oxygen abundance using the calibration formula given in Zaritsky et al. (1994) for the three cases of extinction models. Extinction correction assuming a foreground screen and a homogeneous slab both give $12+\log(\mathrm{O/H}) = 8.80$, while the WTC model results in 8.82, i.e. virtually no change for the small dust extinction of NGC 604. The spectrum of NGC 5461 is affected by a larger dust extinction and from the data by Rayo et al. (1982) we find a difference in oxygen abundance of 0.08 dex between the foreground screen and the 'dusty nucleus' model. This is almost negligible compared to the estimated precision of the oxygen abundance calibration, roughly 0.2 dex (Pagel et al. 1980), although extinction correction by the WTC model will systematically infer higher oxygen abundances. This result makes the widespread use of a simple foreground screen for dereddening justifiable at this magnitude of extinction at least for lines not to far apart. For diagnostic lines with longer separations larger changes are expected, for instance Bautista et al. (1995) find deviations of up to 12 % in nebular abundances in a revaluation of Orion Nebula data with an empirical effective nebular extinction law.

4.1. Spatial variation of the extinction

Two of the H II regions, NGC 5461 and NGC 604, has sufficiently high signal and large extent that the spatial variation of the extinction across an H II region can be studied in greater detail. The E–W aperture (Jul 31) of NGC 5461 has been divided into 5 subapertures of length $3\farcs2$ corresponding to 84 pc at the distance of NGC 5457 and the extracted spectrum from each of them treated in the usual way. In Fig. 5 the optical depths derived in the large aperture and each of the subapertures assuming the foreground geometry are depicted at their positions along the slit on top of the observed flux in one of the Paschen lines, which is less affected by the extinction. As expected, the value of τ_V for the total aperture is close to those found in the central subapertures containing most of the flux with uncertainties increasing outwards. A scatter in τ_V of ~ 0.3 across the region is evident, which could indicate a patchiness of the obscuring dust integrated along the line of sight of this order. A similar behaviour is found by Greve et al. (1989) for the Galactic Orion Nebula.

We also note that τ_V increases towards the edge of the region (subaperture #1 and 4). This can be interpreted as

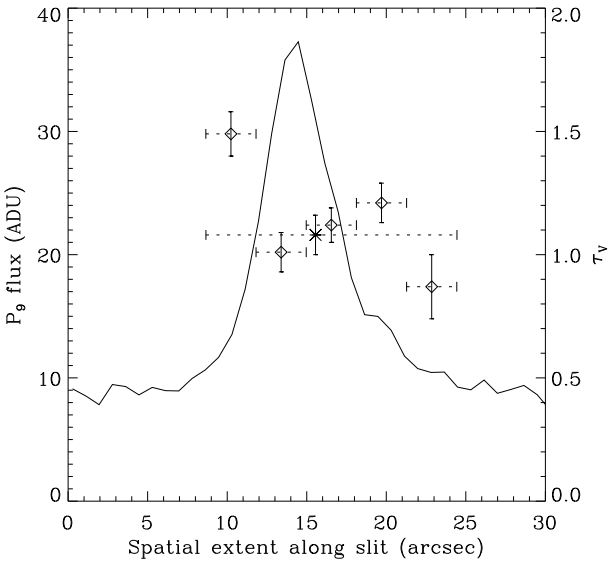

Fig. 5. Spatially resolved optical depth across NGC 5461. The solid line represents observed flux in the spatial direction along the slit in ADU's on the left ordinate at the central wavelength of the P9 emission line. The ⋆ denotes the optical depth given on the right ordinate with associated vertical error bar as derived from the total integrated spectrum. The size of the extraction aperture is shown as the horizontal dotted line. The ◇'s indicate the optical depths found in the 5 subapertures extracted over the short dotted lines

a larger amount of dust residing just outside the brightest part of the H II region possibly due to destruction and outflow of dust in the inner starburst environment. It also fits well with the picture upon which the WTC dusty nucleus simulations are based. Given the uncertainty in modelling the dust geometry discussed above one should, however, be cautious of drawing any firm conclusion on the detailed distribution of the dust.

The separation of the three bright knots observed in the NGC 604 complex are roughly $15''= 50$ pc. From the overlying screen model we find here somewhat smaller variations of τ_V up to 0.1, while Diaz et al. (1987) also found variations in τ_V of the order 0.3 among 5 areas studied in detail. Thus there are signs of variation in the optical depths towards giant extragalactic H II regions on scales smaller than 50 pc most likely attributed to a patchy distribution of the obscuring dust.

4.2. Comparison with previous investigations

The brightest H II regions in NGC 598 and NGC 5457 have been the objective of many extensive studies over the years. In the lower part of Table 3 and 4 independent extinction determinations available in the literature are compiled. The majority are based on the Balmer decrement (Hα/Hβ), but for NGC 5461 two other sources are included. One is derived from the ratio of Pγ/Hβ, while Rosa & Benvenuti (1994) use a different approach fitting population synthesis models to the energy distribution while taking the dust attenuation into account.

A substantial scatter between the different sources is seen, amounting to more than one unit in optical depths for NGC 5461. Part of this can possibly be explained by the different aperture sizes and positions used if the dust distribution is not totally homogeneous and entirely in the foreground, but it may also be related to the problem of deriving the extinction from a pair of lines with only small wavelength separation. The newer results seem to favour the generally high dust extinctions that we derive, but also unexplainable wildly deviating values exist.

Our data display the same tendency as seen in Paper I and also commented by Skillman & Israel (1988), that the derived extinctions increase with increasing wavelength separation. A similar behaviour is found by Bautista et al. (1995) in an analysis of the Orion Nebula, where A_V estimated using the lines of a given recombination line series (Balmer to Brackett) increases with the mean wavelength of that line series. This finding is even based on a value of $R_V = 5.5$, which is appreciable altered from the value of 3.1 valid for the interstellar medium. (With this value the differences would have been more distinct).

This trend correlates with the findings by Viallefond & Goss (1986 and Skillman & Israel (1988) of yet higher values of extinction for NGC 598 and NGC 5457, respectively, when comparing radio continuum emission and Hβ line emission. Both attribute this 'excess' extinction to part of the dust being non-uniformly distributed and/or mixed with the gas. Skillman & Israel (1988) point out that most of the difference appears to be explainable by dust associated with the H II regions, but there is no unambiguous method to distinguish between the two distributions. It is interesting to see that the absorption at Hβ for NGC 595 and NGC 5461 from these two studies when converted to optical depth in V ($\tau_V = 1.4$ and 1.8, respectively) match the effective τ_V of the WTC 'dusty model' in our investigation.

Similarly Caplan & Deharveng (1986) report and average excess in A_V of 0.3 mag for regions in the LMC and attribute this to clumped interstellar dust and scattering dust in a slab near the periphery of the emitting gas. On the other hand Caplan et al. (1996) find in a recent study of the SMC only a few regions with excess extinction and the reddening of the large majority of H II regions being consistent with uniform interstellar extinction.

5. Conclusions

The observations of giant H II regions in the spiral galaxies NGC 598 of NGC 5457 have demonstrated how the dust extinction can be derived on the basis of multiple emission lines from the Balmer and Paschen series in the optical and near-IR regimes obtained simultaneously with ordinary CCD detectors. Although some of these lines can only be observed with larger flux errors the wide wave-

length interval spanned by the lines and the utilisation of the redundancy of the Paschen lines at $\lambda\lambda$8500–9000 Å leads to a small overall uncertainty compared to the use of the two strongest Balmer lines.

Inclusion of lines beyond 1 μm offers a chance to make simple test of the geometrical distribution of emitting source and dust in the light of the common but questionable assumption of a foreground screen. A slab of homogeneous mixture can only match the data points for the H II regions with relative low dust extinction. Generally we can not discriminate between the simple foreground extinction screen and the WTC 'dusty nucleus' model, although signs of deviation from the pure foreground screen are seen at near-IR wavelengths. This is in agreement with Calzetti et al. (1996), who found that the reddening towards starburst regions in 13 galaxies by large can be explained by foreground dust. The choice of extinction model for reddening correction of diagnostic line ratios only has small effects on the derived physical parameters when lines are not widely separated.

It is, however, clearly seen how the foreground screen always yields a lower limit to the dust content and that considerable larger amounts of dust can be present in the 'dusty nucleus' configuration. A more definitive discrimination between various geometries, possibly including patchiness, and assessment of the actual dust content will need investigations at even longer wavelengths in combination with optical lines (Puxley & Brand 1994; Genzel et al. 1995; Calzetti et al.1996) and more refined modelling (Witt & Gordon 1996). While a lot can be learned from high-S/N observations of Pγ obtainable with the high quantum efficiency of the new generation of CCD's, it is desirable to have data on emission lines further out in the near-IR, e.g. Pβ, Brγ, Brα, which can not be observed with the same instruments as the blue optical lines. The kind of studies presented in this paper can serve to bridge the two wavelength ranges.

One obvious result from the present study is the demonstration of a spatial variation in the optical depth towards the emission regions of the order 0.2–0.3 on small angular scales. More detailed investigations of one of the H II regions suggest that the extinction has it highest value at or close to the edge of the region. This can explain at least some of the disagreement in the quoted extinction of H II regions by different authors. It also emphasizes the importance of sampling exactly the same slit position and aperture size if combining data from different observations, and the care that most be taken when comparing physical parameters from miscellaneous sources in the literature.

References

Bautista M.A., Pogge R.W., DePoy D.L., 1995, ApJ 452, 685
Boissé P., 1990, A&A 228, 483
Boulesteix J., Courtès G., Laval A., Monnet G., Petit H., 1974, A&A 37, 33
Bruzual G.A., Magris G.C., Calvet N., 1988, ApJ 333, 673
Calzetti D., Kinney A.L., Storchi-Bergmann T., 1994, ApJ 429, 582
Calzetti D., Kinney A.L., Storchi-Bergmann T., 1996, ApJ 458, 132
Caplan J., Deharveng L., 1986, A&A 155, 297
Caplan J., Ye T., Deharveng L., Turtle A.J., Kennicutt Jr. R.C., 1996, A&A 307, 403
Cardelli J.A., Clayton G.C., Mathis J.S., 1989, ApJ 345, 245
de Vaucouleurs G., de Vaucouleurs A., Corwin H.G. et al., 1991, Third Reference Catalogue of Bright Galaxies, Springer-Verlag, New York
Díaz A.I., Terlevich E., Pagel B.E.J., Vilchez J.M., Edmunds M.G., 1987, MNRAS 226, 19
Disney M., Davies J., Phillipps S., 1982, MNRAS 239, 939
Evans R., 1996, Probing the optical depth of spirals using multi-waveband observations. In: Minnitti D., Rix H. (eds.) Spiral galaxies in the near-IR. Springer, Berlin, p. 283
Filippenko A.V. 1982, PASP 94, 715
French H.B., 1980, ApJ 240, 41
Genzel R., Weitzel L., Tacconi-Garman L.E. et al., 1995, ApJ 444, 129
Greve A., McKeith C.D., Barnett E.W., Götz M., 1989, A&A 215, 113
Greve A., Castles J., McKeith C.D., 1994, A&A 284, 919
Hodge P.W., Gurwell M., Goldader J.D., Kennicutt Jr. R.C., 1990, ApJS 73, 661
Hummer D.G., Storey P.J., 1987, MNRAS 224, 801
Jansen R.A., Knapen J.H., Beckman J.E., Peletier R.F., Hes R., 1994, MNRAS 270, 373
Kennicutt Jr. R.C., Garnett D.R., 1996, ApJ 456, 504
Kwitter K.B., Aller L.H., 1981, MNRAS 195, 939
McCall M.L., Rybski P.M., Shields G.A., 1985, ApJS 57, 1
Melnick J., Moles M., Terlevich R., Garcia-Pelayo J., 1987, MNRAS 226, 849
Natta A., Panagia N., 1984, ApJ 287, 228
Oke J.B., Gunn J.E., 1983, ApJ 266, 713
Osterbrock D.E., 1989, Astrophysics of Gaseous Nebulae and Active Galactic Nuclei, University Science Books, California.
Pagel B.E.J., Edmunds M.G., Smith G., MNRAS 193, 219
Peimbert S., Spinrad H., 1970, ApJ 159, 809
Petersen L., Gammelgaard P., 1996, A&A 308, 49 (Paper I)
Puxley P.J., Brand P.W.J.L., 1994, MNRAS 266, 431
Rayo J.F., Peimbert M., Torres-Peimbert S., 1982, ApJ 255, 1
Rosa M.R., Benvenuti P., 1994, A&A 291, 1
Skillman E.D., Israel F.P., 1988, A&A 203, 226
Smith H.E., 1975, ApJ 199, 591
van Driel W., Valentijn E.A., Wesselius P.R., Kussendrager D., 1995, A&A 298, L41
Viallefond F., Goss W.M., 1986, A&A 154, 357
Vílchez J.M., Pagel B.E.J., Díaz A.I., Terlevich E., Edmunds M.G., 1988, MNRAS 235, 633
Witt A.N., Thronson Jr. H.A., Capuano Jr. J.M., 1992, ApJ 393, 611 (WTC)
Witt A.N., Lindell R.S., Block D.L., Evans R., 1994, ApJ 427, 227
Witt A.N., K.D. Gordon, 1996, ApJ 463, 681

Zaritsky D., Kennicutt Jr. R.C., Huchra J.P. 1994, ApJ 420, 87

This article was processed by the author using Springer-Verlag LaTeX A&A style file *L-AA* version 3.